The Astrophysical Journal, 613:631–645, 2004 October 1

THE STRUCTURE AND EVOLUTION OF EARLY COSMOLOGICAL H II REGIONS

Tetsu Kitayama
Department of Physics, Toho University, Funabashi, Chiba 274-8510 Japan; kitayama@ph.sci.toho-u.ac.jp

Naoki Yoshida
Department of Physics, Nagoya University, Chikusa-ku, Nagoya 464-8602; and National Astronomical Observatory of Japan, Mitaka, Tokyo 186-8588, Japan

Hajime Susa
Department of Physics, Rikkyo University, Toshimaku, Tokyo 171-8501, Japan

and

Masayuki Umemura
Center for Computational Sciences, University of Tsukuba, Tsukuba 305-8577, Japan
Received 2004 March 2; accepted 2004 June 15

ABSTRACT

We study the formation and evolution of H II regions around the first stars formed at redshifts $z = 10-30$. We use a one-dimensional Lagrangian hydrodynamics code that self-consistently incorporates radiative transfer and nonequilibrium primordial gas chemistry. The star-forming region is defined as a spherical dense molecular gas cloud with a Population III star embedded at the center. We explore a large parameter space by considering, as plausible early star-forming sites, dark matter halos of mass $M_{\rm halo} = 10^5-10^8\ M_\odot$, gas density profiles with a power-law index $w = 1.5-2.25$, and metal-free stars of mass $M_{\rm star} = 25-500\ M_\odot$. The formation of the H II region is characterized by initial slow expansion of a weak D-type ionization front near the center, followed by rapid propagation of an R-type front throughout the outer gas envelope. We find that the transition between the two front types is indeed a critical condition for the complete ionization of halos of cosmological interest. In small-mass ($\lesssim 10^6\ M_\odot$) halos, the transition takes place within a few 10^5 yr, yielding high escape fractions (>80%) of both ionizing and photodissociating photons. The gas is effectively evacuated by a supersonic shock, with the mean density within the halo decreasing to $\lesssim 1$ cm^{-3} in a few million years. In larger mass ($\gtrsim 10^7\ M_\odot$) halos, the ionization front remains to be of D-type over the lifetime of the massive star, the H II region is confined well inside the virial radius, and the escape fractions are essentially zero. We derive an analytic formula that reproduces well the results of our simulations for the critical halo mass below which the gas is completely ionized. We discuss immediate implications of the present results for the star formation history and early reionization of the universe.

Subject headings: cosmology: theory — early universe — H II regions — radiative transfer

Online material: color figures

1. INTRODUCTION

The emergence of the first-generation stars has significant impacts on the thermal state of the intergalactic medium (IGM) in the early universe. The initially neutral cosmic gas is photoionized and photoheated by radiation from the first stars. This so-called radiative feedback from the first stars is of considerable cosmological interest. It can not only self-regulate the first star formation, but also affect the formation and evolution of protogalaxies.

Theories based on cold dark matter (CDM) predict that the first cosmological objects form when small-mass ($\sim 10^6\ M_\odot$) dark halos assemble at redshifts $z = 20-30$ (Couchman & Rees 1986; Tegmark et al. 1997; Abel et al. 1998; Yoshida et al. 2003a). Stars formed in these pregalactic objects may have substantially contributed to cosmic reionization. Recent measurement of the large Thomson optical depth by the *Wilkinson Microwave Anisotropy Probe* (*WMAP*) satellite indicates that the universe was reionized at an epoch as early as $z \sim 17$ (Kogut et al. 2003; Spergel et al. 2003), supporting the above notion that the first-generation stars formed at $z \gtrsim 20$. Theoretical studies of the processes of cosmic reionization by stellar sources suggest that reionization proceeds first by the formation of individual H II regions around radiation sources (galaxies) and then by percolation of the growing H II bubbles (Gnedin & Ostriker 1997; Ricotti et al. 2002; Sokasian et al. 2004). The shape and the extension of the individual H II regions critically determine the global topology of the ionized regions in a cosmological volume at different epochs during reionization.

Studies on the formation of H II regions in dense gas clouds date back to the seminal work by Strömgren (1939). Since then the structure of H II regions and the interaction with the surrounding medium have been extensively studied (see Yorke 1986 for a review). An important advance has been made by Franco et al. (1990), who considered realistic conditions in which the initial gas density profile is given by a power law. Franco et al. showed that a hydrodynamic shock effectively sweeps the ambient medium into a thin shell and the gas density profile is significantly modified from the initial power-law shape. Shu et al. (2002) obtained the self-similar solutions for the expansion of self-gravitating H II regions. On cosmological backgrounds, Shapiro & Giroux (1987) studied the evolution of the cosmological Strömgren sphere around luminous quasars in an expanding universe. Ricotti & Shull

(2000) computed the UV photon consumption in small-mass halos to estimate the photon escape fraction. Their calculations, however, do not include the hydrodynamic response of the photoheated gas and are not adequate to address the dynamical evolution of H II regions. More recently, Whalen et al. (2004) carried out a numerical simulation of ionization front (I-front) propagation starting from a realistic initial density profile for the first star-forming cloud. Whalen et al. found that the escape fraction of ionizing photons is close to unity in a particular case with halo mass $7 \times 10^5\ M_\odot$ at $z \sim 20$. It is by no means trivial if such high escape fraction is achieved for different masses and redshifts.

In the present paper, we study the evolution of H II regions around Population III stars for a wide range of halo mass, redshift, and gas density profile. Specifically, we consider an "inside-out" situation, where the central source ionizes the surrounding gas and drives a supersonic gas flow outward. While the overall configuration of our simulations may appear similar to those in conventional studies on H II regions, we have several critical ingredients relevant to the case of early generation star formation:

1. Gravitational force exerted by the host dark matter halo.
2. Radiation force by the central star.
3. Radiative transfer of UV photons.
4. Chemical reactions, including formation and destruction of hydrogen molecules.
5. Radiative cooling and heating processes, including inverse Compton cooling, which is particularly important at $z > 10$.

Our inside-out simulations are complementary to a number of works that focused on radiative feedback from an external field (Umemura & Ikeuchi 1984; Rees 1986; Bond et al. 1988; Efstathiou 1992; Thoul & Weinberg 1996; Kepner et al. 1997; Barkana & Loeb 1999; Kitayama & Ikeuchi 2000; Susa & Umemura 2000, 2004; Kitayama et al. 2000, 2001; Shapiro et al. 2003, 2004). While external radiation can easily ionize and blow away the outer envelope of gas clouds, photoevaporation proceeds less effectively in the densest central part. Shapiro et al. (2004) indeed show that evaporation of an initially hydrostatic minihalo ($\sim 10^6\ M_\odot$) takes about 100 million years when irradiated by a luminous source at a distance of $\sim$1 Mpc. At the very center of the halo, self-shielding and dynamical infall of the gas can prevent complete evaporation and promote star formation (Kitayama et al. 2001; Susa & Umemura 2004). The subsequent evolution of the gas cloud will then be largely regulated by the feedback from the central star. As will be shown in the present paper, ionization of the ambient gas by an internal source is more rapid than that by the external radiation because of the greater incident radiation flux and the presence of the gas-density gradient.

The final state of the ionized gas near the central region is of particular interest in the study of the first supernova explosions (e.g., Bromm et al. 2003; Wada & Venkatesan 2003). The subsequent evolution of the ionized gas has also an important implication for the formation of protogalaxies (Oh & Haiman 2003). For the gas clouds hosted by minihalos with mass $\sim 10^6\ M_\odot$, one may naively expect that the gas is completely photoionized and eventually photoevaporated, because the virial temperature of the system is much lower than the characteristic temperature of photoionized gas. On the other hand, larger dark matter halos generate a deeper gravitational potential well, and thus it can effectively trap the hot, ionized gas within a small radius, rather than letting it move outward by pressure. The actual situation is likely to be far more complicated, depending upon the luminosity and the spectrum of the radiation source, and also on the initial gas density profile. It is clearly important to make reliable predictions, under various physical conditions, as to how the gas is redistributed by radiation from the central star.

Throughout the present paper, we work with a Λ-dominated CDM cosmology with the matter density $\Omega_M = 0.3$, the cosmological constant $\Omega_\Lambda = 0.7$, the Hubble constant $h = 0.7$, and the baryon density $\Omega_B = 0.05$.

2. THE SIMULATIONS

2.1. *Numerical Scheme*

We study the evolution of H II regions around a primordial star using the radiation-hydrodynamics code of Kitayama et al. (2001). The code employs the second-order Lagrangian finite-difference scheme in spherically symmetric geometry (Bowers & Wilson 1991; see also Thoul & Weinberg 1995). It treats self-consistently gravitational force, hydrodynamics, nonequilibrium chemistry of primordial gas, and the radiative transfer of UV photons. In the present paper, we further incorporate the radiation force. We also adopt an artificial viscosity formulation of Caramana et al. (1998), designed to distinguish between shock-wave and uniform compression using an advection limiter.

The basic equations are given by

$$\frac{dm}{dr} = 4\pi r^2 \rho, \tag{1}$$

$$\frac{d^2 r}{dt^2} = -4\pi r^2 \frac{dp}{dm} - \frac{GM_{\rm tot}(<r)}{r^2} + f_{\rm rad}, \tag{2}$$

$$\frac{du}{dt} = \frac{p}{\rho^2}\frac{d\rho}{dt} + \frac{\mathcal{H} - \mathcal{L}}{\rho}, \tag{3}$$

$$p = \frac{2}{3}\rho u, \tag{4}$$

where r, m, ρ, p, u, and $M_{\rm tot}(<r)$ are the radius, mass, density, pressure, internal energy per unit mass, and the total mass inside r, respectively. The radiative heating and cooling rates per unit volume, $\mathcal{H}$ and $\mathcal{L}$, and the radiation force per unit mass, $f_{\rm rad}$, depend on the solutions of the radiative transfer equation and the chemical reactions. We therefore take the following procedure at each time step we advance with the momentum equation (eq. [2]).

First, the direction- and frequency-dependent radiative transfer is worked out as described in detail in Appendix A. We solve both absorption and emission of ionizing ($\geq$13.6 eV) photons and take account of self-shielding of H_2 against the Lyman-Werner (LW; 11.2–13.6 eV) band photons following Draine & Bertoldi (1996). This yields the UV heating rate $\mathcal{H}$ and the radiation force $f_{\rm rad}$, together with the coefficients for photoioniziation of H, photodissociation of H_2 and H_2^+, and photodetachment of H^-. The obtained coefficients are used in the chemical reaction network mentioned below.

Second, nonequilibrium chemical reactions are solved by an implicit scheme developed by Susa & Kitayama (2000) for the species e, H, H^+, H^-, H_2, and H_2^+.[1] Unless otherwise stated,

[1] In the present paper, we consider only the hydrogen component of the IGM. Including helium will raise the temperature of photoionized gas and may affect the overall evolution of H II regions. This point will be discussed in § 3.3.

TABLE 1
PROPERTIES OF METAL-FREE STARS (SCHAERER 2002)

$M_{\rm star}$ ($M_\odot$)	$t_{\rm life}$ (Myr)	$T_{\rm eff}$ (K)	$\dot{N}_{\rm ion}$ (s^{-1})
500	1.90	1.07×10^5	6.80×10^{50}
200	2.20	9.98×10^4	2.62×10^{50}
80	3.01	9.33×10^4	7.73×10^{49}
25	6.46	7.08×10^4	7.58×10^{48}

the reactions and the rates are taken from the compilation of Galli & Palla (1998).

Finally, the energy equation (eq. [3]) is solved including UV heating and radiative cooling due to collisional ionization, collisional excitation, recombination, thermal bremsstrahlung, Compton scattering with the cosmic microwave background (CMB) radiation, and rovibrational excitation of H_2. The atomic cooling rates are taken from the compilation of Fukugita & Kawasaki (1994), and the molecular cooling rates are from Galli & Palla (1998).

The above procedure is repeated iteratively until the abundance of each species and the internal energy in each mesh converge within an accuracy of 0.1%. We have validated the accuracy of our code by carrying out a suite of conventional tests. The results of a "Strömgren sphere" test are presented in Appendix B.

2.2. *Central Source*

At the center of a gas cloud, we place a metal-free Population III star. Its parameters are taken from Schaerer (2002) and listed in Table 1. We vary the stellar mass, denoted by $M_{\rm star}$, over the range 25–500 $M_\odot$ and approximate the spectrum by a blackbody with the effective temperature $T_{\rm eff}$. The luminosity is normalized so that the number of ionizing photons emitted per second, $\dot{N}_{\rm ion}$, matches the time-averaged photon flux given in Table 4 of Schaerer (2002). For simplicity, we neglect its spectral evolution. Unless stated otherwise, the simulations are performed during the main-sequence lifetime, $t_{\rm life}$, of the central star.

2.3. *Initial Conditions*

We assume that a star-forming gas cloud is embedded in a dark matter halo with the NFW density profile (Navarro et al. 1997):

$$\rho_{\rm DM} \propto \frac{1}{x(1+x)^2}, \tag{5}$$

where $x = r/r_s$ is the radius normalized by the scale radius r_s. We follow Bullock et al. (2001) to determine r_s for a halo with total mass $M_{\rm halo}$ collapsing at redshift z_c, by extrapolating their formula to the lower halo masses and the higher redshifts. The dark matter density is normalized so that the dark matter mass within the virial radius is equal to $M_{\rm DM} = (1 - \Omega_B/\Omega_M)M_{\rm halo}$. We assume that the dark matter density profile remains unchanged, since the halo dynamical timescale is much longer than the lifetime of the massive star.

For the gas in the halo, we adopt a power-law density profile

$$\rho \propto r^{-w} \tag{6}$$

and vary the index w from 1.5 to 2.25. This power-law profile is motivated by the results of recent three-dimensional simulations of the primordial gas cloud formation (Abel et al. 2002; Yoshida et al. 2003a) that show that the gas density profile around the first star-forming regions is well described with $w \sim 2$ over a wide range of radii. The gas density is normalized so that the total gas mass within the halo virial radius is equal to $M_{\rm gas} = (\Omega_B/\Omega_M)M_{\rm halo} - M_{\rm star}$. We determine the radius of the innermost gas shell $r_{\rm in}$ such that

$$\bar{n}_{\rm H}(<r_{\rm in}) = 10^6 \ {\rm cm}^{-3}, \tag{7}$$

where $\bar{n}_{\rm H}(<r)$ is the average hydrogen number density within r. This density is comparable to that of primordial molecular cloud cores or fragments found in numerical simulations (Abel et al. 2002; Bromm et al. 2002; Nakamura & Umemura 2002), and it gives $r_{\rm in}$ sufficiently smaller than the characteristic size of the simulated halos. Our primary interest hence lies in the propagation of UV photons after they escape out of the dense molecular cloud.[2] If a gas shell falls below $0.5r_{\rm in}$, it is moved to the center and ignored in the rest of the simulation, except in the calculation of the gravitational force. In order to trace the propagation of an I-front for a sufficiently long time, the outer boundary is taken at 1–3 times the virial radius depending on the run. The gas shells are initially spaced such that the shell mass increases by a constant ratio, typically $\sim$1%, between the adjacent shells. We have checked that a total of 300 radial bins from the center to the outermost shell is sufficient to produce converged results. Since the star-forming clouds are likely to be in the course of collapse, we assign the initial velocity

$$v_{\rm init}(r) = -\sqrt{\frac{2GM_{\rm tot}(<r)}{r}}. \tag{8}$$

We assume that the gas is initially isothermal with temperature $T_{\rm init}$, given by the *minimum* of the virial temperature $T_{\rm vir}$ and a reference temperature $T_{\rm min}$. We take $T_{\rm min} = 500$ K, corresponding to the gas that has cooled by molecular hydrogen cooling. The final results are found to be insensitive to the choice of $T_{\rm min}$, because as long as $T_{\rm min} \ll 10^4$ K, the gas is initially almost neutral and the opacity to ionizing photons is very large.

The initial abundances are taken to be consistent with the above choice of the initial temperature based on the hydrodynamical simulations of Kitayama et al. (2001); $X_e = 10^{-4}$, $X_{\rm H^-} = 10^{-10}$, $X_{\rm H2} = 10^{-3}$, and $X_{\rm H2^+} = 10^{-12}$, where $X_i \equiv n_i/n_{\rm H}$ is the fraction of the species i with respect to the total number of hydrogen atoms.

3. RESULTS

3.1. *I-Front Propagation*

We first describe in detail the results of our fiducial runs with $M_{\rm star} = 200\ M_\odot$, $w = 2.0$, and $z_c = 20$. Simulations with

[2] The infalling envelope may prevent the escape of UV photons from dense protostellar clouds. Omukai & Inutsuka (2002) showed that, in spherically symmetric cases, H II regions around a massive star cannot expand under significant mass accretion. Mass accretion onto a dense protostellar cloud, however, could occur along an aspherical disk due to its angular momentum. For disklike geometries, escape of the UV photons from the proximity of the massive star will be greatly enhanced than in the spherically symmetric case. In the present paper, we focus on such cases that the UV photons could successfully escape out of a protostellar disk and propagate through the surrounding halo.

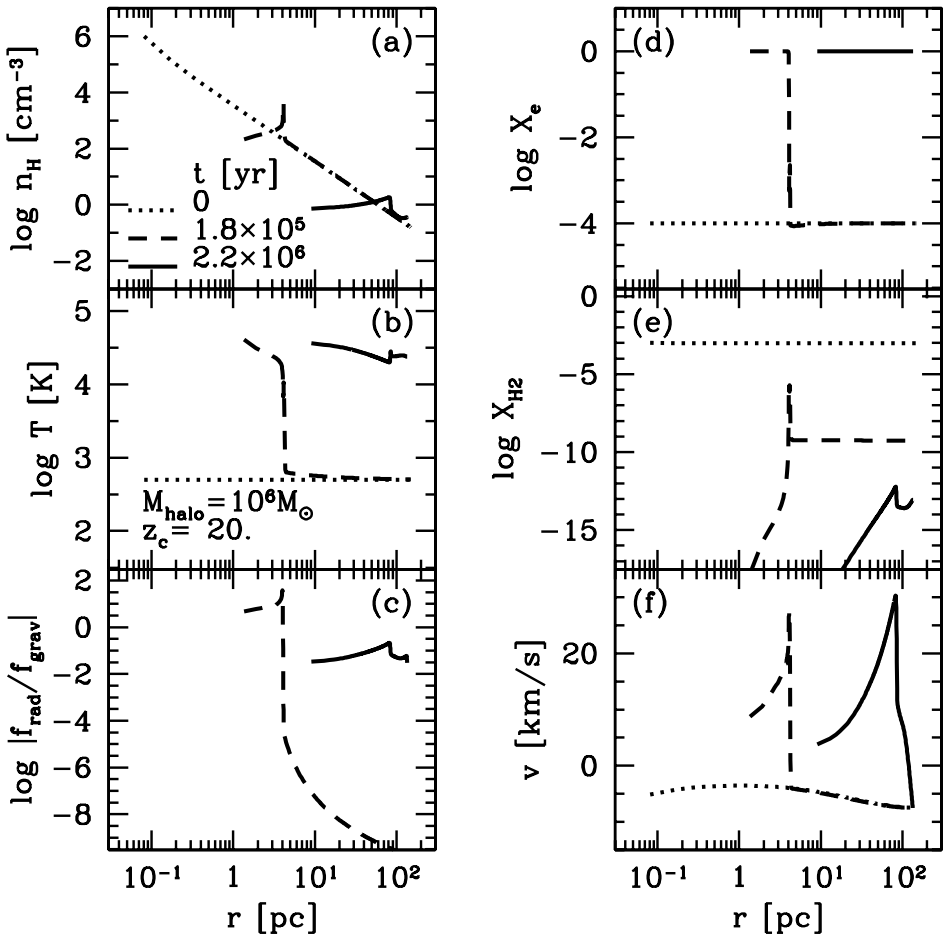

FIG. 1.—Structure of an H II region around a massive star with $M_{\rm star} = 200\ M_\odot$ inside a halo with $M_{\rm halo} = 10^6\ M_\odot$ and $w = 2.0$ at $z_c = 20$. Radial profiles are shown at $t = 0$ (*dotted lines*), 1.8×10^5 yr (*dashed lines*), and 2.2×10^6 yr (*solid lines*) for (*a*) hydrogen density, (*b*) temperature, (*c*) ratio of radiation force to gravitational force, (*d*) electron fraction, (*e*) H_2 fraction, and (*f*) radial velocity. [*See the electronic edition of the Journal for a color version of this figure.*]

other sets of parameters are also carried out, and the results are presented in due course.

Figure 1 shows the structure of the H II region at $t = 0$ (initial), 1.8×10^5, and 2.2×10^6 yr for a low-mass case with $M_{\rm halo} = 10^6\ M_\odot$. The evolution in the early stage is characterized by the propagation of a weak D-type front into the surroundings; shock precedes the I-front. Because of the steep density gradient, the I-front eventually overtakes the shock and changes into R-type. The transition takes place at $t \sim 3 \times 10^5$ yr (see also Fig. 3 and discussions below). In this so-called champagne phase, the low-density envelope is promptly ionized (Welter 1980) and the gas temperature rises to a few times 10^4 K. As the shock propagates at the speed $\sim$30 km s^{-1}, it reaches $\sim$70 pc within the lifetime of the massive star, $t_{\rm life} = 2.2$ Myr.

The spatial resolution of the present simulation is sufficient to resolve the cooling layer behind the shocks; e.g., the I-front at $t = 1.8 \times 10^5$ yr in Figure 1 is resolved with more than 10 shells. We have also performed the runs with halving and doubling the gas shell numbers and confirmed that the results are almost identical.

We notice that there appears a thin shell of H_2 just in front of the H II region (Fig. 1*e*), as pointed out by Ricotti et al. (2001). This is due to a positive feedback on the H_2 formation by an enhanced electron fraction at the temperature below 10^4 K. As the H II region expands, the temperature in the shell exceeds 10^4 K and H_2 molecules are dissociated by collisions with ions. There still appears a new H_2 shell in front of the I-front, but in a different position (both Eulerian and Lagrangian) from the previous one. The H_2 shell is thus likely to be short-lived as a result of I-front propagation. There may also be a case that the H_2 formation is promoted after the central star fades away and the gas cools to temperatures below 10^4 K. Such a possibility will be explored later in this subsection.

Interestingly, the radiation force dominates over the gravitational force inside the H II region when the I-front radius is smaller than $\sim$30 pc (Fig. 1*c*). This value is a factor of $\sim$4 smaller than that indicated by Haehnelt (1995), and is easily accounted for by the fact that there is about 3–5 times more mass contributed by dark matter than baryons near the center in our simulations.

For a higher mass halo with $10^7\ M_\odot$, illustrated in Figure 2, the outward gas motion near the center is eventually reverted to an inflow. Correspondingly, the shock radius starts *decreasing*. This reversion is explained by a combination of the deep gravitational potential well near the halo center and the infall of the envelope gas. Notice that the ionization fraction decreases sharply at $r \sim 1$ pc and $t = 1.8 \times 10^5$ yr. The infalling material piles on the shock front, enhancing recombination (Fig. 2*d*). This is, however, just in a transition phase; the piled gas rapidly falls back to the center. Thereafter, the H II region is kept trapped within a few parsec radius because the gas density remains high ($\gtrsim 10^4$ cm^{-3}) and recombination balances photoionization. We have carried out a simulation for

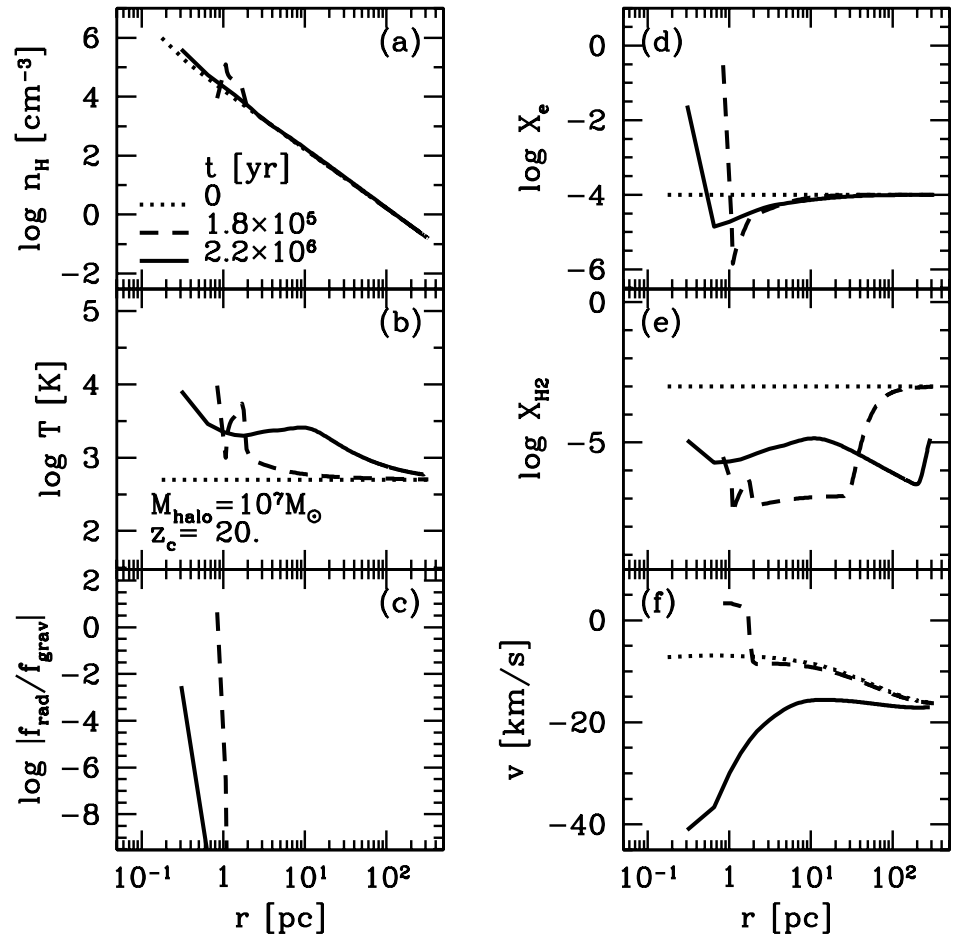

FIG. 2.—Same as Fig. 1, except that the halo mass is $M_{\rm halo} = 10^7\ M_\odot$. [*See the electronic edition of the Journal for a color version of this figure.*]

the same set of parameters, but assuming that the gas is initially static. Even in this case, the D-type front maintains over $t_{\rm life} = 2.2$ Myr and reaches only $\sim$40 pc, still well inside the virial radius.

Figure 3 further compares the time evolution in the two cases presented in Figures 1 and 2. For definiteness, we take the shock front radius at the peak of gas density and the I-front radius at the position with $X_{\rm H\,I} = 0.1$. The mass-weighted mean fractions of H I and H_2 are computed within the virial radius $r_{\rm vir}$. For $M_{\rm halo} = 10^6\ M_\odot$, the I-front detaches from the shock at $t \sim 3 \times 10^5$ yr and then propagates rapidly, exceeding the halo virial radius. The halo gas is almost completely ionized in the first few hundred thousand years, and then a large fraction of ionizing and the LW photons can escape from the halo. For $M_{\rm halo} = 10^7\ M_\odot$, on the other hand, the I-front *stalls* at $t \sim 3 \times 10^5$ yr and then moves back inward. A large fraction of the gas is neutral, but the H_2 fraction drops by 3 orders of magnitude from the initial value because the LW photons can penetrate further than ionizing ones.

The evolution after the lifetime of the central star ($t > 2.2$ Myr) is also plotted in Figure 3. In the $10^6\ M_\odot$ case, if the central star simply fades away without triggering a supernova explosion (as is assumed in our calculations), the gas is undisturbed and quickly recombines (Fig. 3*c*) and reforms molecules (Fig. 3*d*). The large ionization fraction within the H II region can accelerate production of hydrogen molecules through H^- formation. The shock front continues expanding until it dissipates kinetic energy.

Alternatively, if the central star turns into a supernova, it will generate a blast wave, which runs through the ambient gas. A quantity that is of particular importance in such a case is the final density of the evacuated gas near the center (see § 4 for more details). It is in fact primarily determined by the host halo mass. In the low-mass case ($M_{\rm halo} = 10^6\ M_\odot$), the central gas density drops to $\sim$1 cm^{-3} at $t = 2.2$ Myr. In the high-mass case ($M_{\rm halo} = 10^7\ M_\odot$), the central density remains much higher at $\gtrsim 10^4$ cm^{-3}. The threshold between the two cases closely follows that of the escape fraction of ionizing photons described in § 3.3.

3.2. *Photon Escape Fraction*

A useful output of our simulations is the escape fractions of ionizing photons and the LW photons from a halo. The former is of particular significance in terms of early reionization of the universe (e.g., Yoshida et al. 2003b; Sokasian et al. 2004; Whalen et al. 2004), while the latter quantifies the efficiency of the so-called negative feedback on subsequent star formation (Haiman et al. 1997; Omukai & Nishi 1999).

In Figures 4–6 we plot the escape fractions, averaged over the lifetime of the central star, as a function of halo mass for various choices of $M_{\rm star}$, w, and z_c. In the case of $M_{\rm star} = 25\ M_\odot$ (Fig. 4), for instance, the escape fraction of ionizing photons $f_{\rm esc}^{\rm ion}$ is below 0.5 over the range of $M_{\rm halo}$ we consider. For $M_{\rm star} = 200\ M_\odot$, on the other hand, $f_{\rm esc}^{\rm ion}$ is close to unity at $M_{\rm halo} < 10^6\ M_\odot$ but drops sharply at $M_{\rm halo} \sim 2 \times 10^6\ M_\odot$. There appears to be a critical mass of the host halo above which

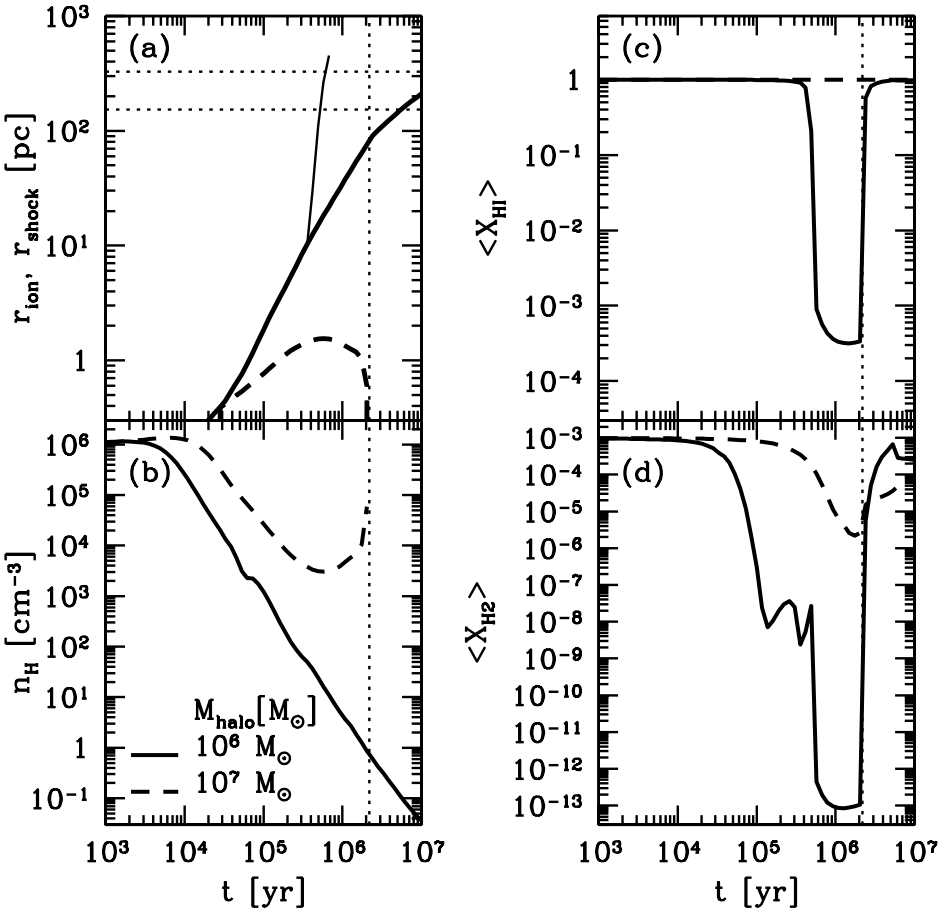

FIG. 3.—Evolution of (*a*) shock front radius (*thick lines*) and I-front radius (*thin lines*, whenever separated from the shock), (*b*) central hydrogen density, (*c*) mean H I fraction within r_{vir}, and (*d*) mean H_2 fraction within r_{vir}, for halos with $M_{halo} = 10^6$ (*solid lines*) and $10^7\ M_\odot$ (*dashed lines*) shown in Figs. 1 and 2, respectively. Horizontal dotted lines denote virial radii of halos with $M_{halo} = 10^6\ M_\odot$ and $10^7\ M_\odot$, while the vertical one indicates the lifetime of the central star with $M_{star} = 200\ M_\odot$. [*See the electronic edition of the Journal for a color version of this figure*.]

f_{esc}^{ion} is essentially zero. For the escape fraction of the LW photons f_{esc}^{LW}, similar features are found with a slightly larger critical mass, because the LW photons are harder to shield than ionizing photons. A plateau and a small dip at $f_{esc}^{LW} \sim 0.1$ are real; a minor leakage of ionizing photons causes a weak positive feedback on H_2 formation by enhancing electron fraction (Haiman et al. 1996).

Figure 5 indicates that a steeper density profile leads to smaller escape fractions. This is because, for given gas mass in a halo, a steeper profile results in higher density near the center. The I-front propagation is then prevented at early stages owing to the higher recombination rate. Similarly, an earlier collapse epoch implies a denser, compact halo, from which escape fractions are smaller (Fig. 6).

Strictly speaking, the self-shielding function of the LW photons we adopt (Drain & Bertoldi 1996) is derived for the stationary gas. In the presence of supersonic flows, the photons may Doppler-shift out of or into particular lines in the LW band. A detailed account for these effects requires precise treatment of the line transfer incorporating velocity and temperature structures of the gas, which is beyond the scope of the present paper. Our results on f_{esc}^{LW} should therefore be regarded as a minimal estimation for the true value.

3.3. *Critical Mass for Photon Escape*

Figure 7 summarizes the degree of radiative feedback and photon escape as a function of M_{star}, w, and z_c. Low-mass halos are ionized promptly after the onset of the central star, resulting in high escape fractions of both ionizing and the LW photons. On the other hand, the H II regions are heavily confined and the escape fractions are essentially zero in high-mass halos. For intermediate halos, a significant fraction of the LW photons can escape from the halos while the ionizing photons are trapped. Figure 7 further indicates that the threshold mass scale for the escape of ionizing photons, as a function of M_{star}, w, and z_c, is well reproduced by the following analytic estimation.

Over the range of gas density gradient we consider ($1.5 < w < 2.25$), the shock velocity is a weak function of w and given roughly by 25–35 km s^{-1} (see also Shu et al. 2002). For the low-mass halos considered in this paper, the gravitational infall velocity is 5–10 km s^{-1}. Within the lifetime of the central star t_{life}, the D-type front can then reach the distance

$$l_D = 20\left(\frac{t_{life}}{10^6\ \mathrm{yr}}\right)\left(\frac{v_D}{20\ \mathrm{km\ s^{-1}}}\right)\ \mathrm{pc}, \qquad (9)$$

where v_D is the expansion velocity of a D-type front. This is in general much smaller than the virial radius of a halo in consideration:

$$r_{vir} = 160\left(\frac{M_{halo}}{10^6\ M_\odot}\right)^{1/3}\left(\frac{1+z_c}{20}\right)^{-1}\ \mathrm{pc}, \qquad (10)$$

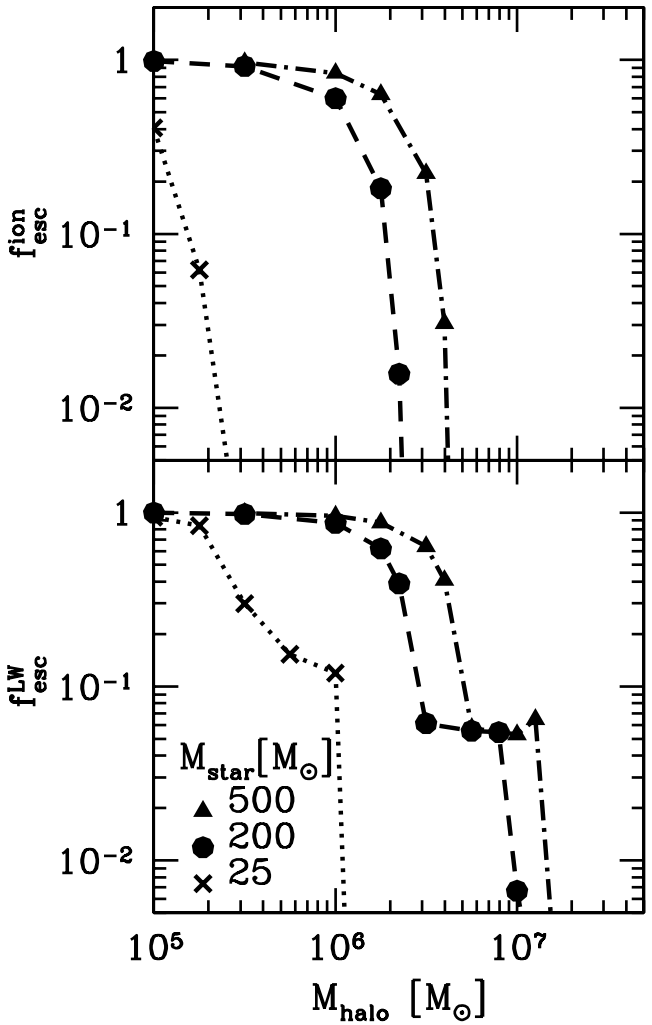

FIG. 4.—Escape fractions of ionizing photons (≥13.6 eV, *top panel*) and the LW photons (11.2–13.6 eV; *bottom panel*) vs. $M_{\rm halo}$. Symbols denote stellar masses of $M_{\rm star} = 500\ M_\odot$ (*triangles*), 200 $M_\odot$ (circles) and 25 $M_\odot$ (*crosses*). A plateau and a small dip at $f_{\rm esc}^{\rm LW} \sim 0.1$ are due to a weak positive feedback on H_2 formation by an enhanced electron fraction. [*See the electronic edition of the Journal for a color version of this figure.*]

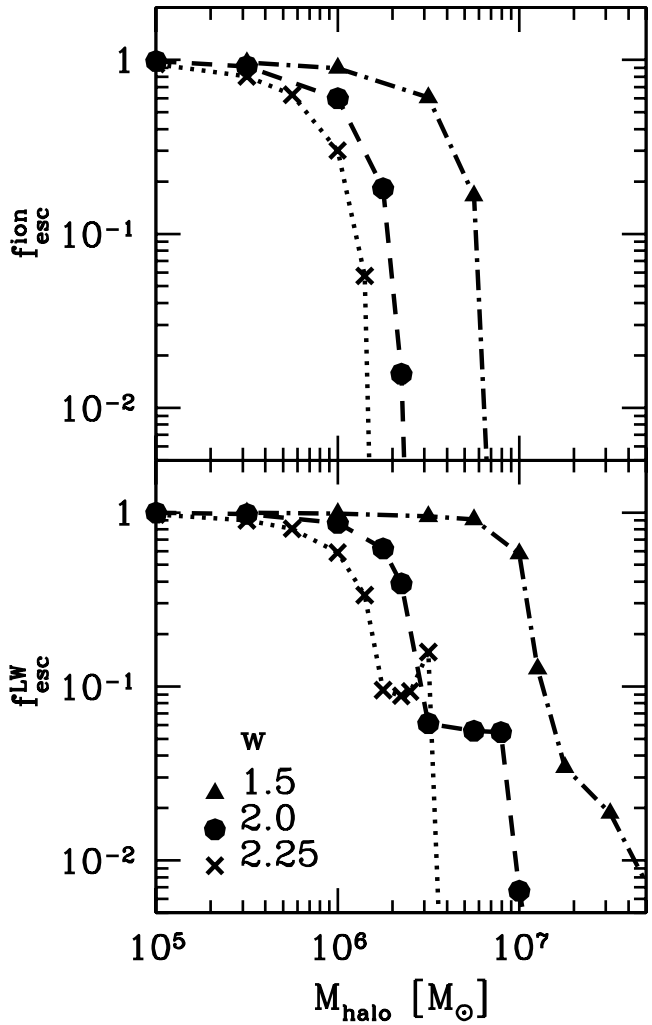

FIG. 5.—Same as Fig. 4, except that symbols denote gas density slopes of $w = 1.5$ (*triangles*) 2.0 (*circles*), and 2.25 (*crosses*). [*See the electronic edition of the Journal for a color version of this figure.*]

applicable to current cosmology at $z \gtrsim 10$. It is therefore necessary for the I-front to become R-type in order to ionize the whole halo.

As shown in Figure 1, the gas density inside the shock front r_s is nearly constant and is approximated by the average density within r_s:

$$n_s = \frac{3}{3-w} n_i(r_s) = 0.39 \left(\frac{1+z_c}{20}\right)^3 \left(\frac{r_s}{r_{\rm vir}}\right)^{-w} {\rm cm}^{-3}, \quad (11)$$

where $n_i(r_s)$ is the initial gas density at r_s, normalized by the condition that the total gas mass within $r_{\rm vir}$ is equal to $M_{\rm halo}\Omega_B/\Omega_M$. One can then define the Strömgren radius (Strömgren 1939) corresponding to n_s as

$$r_{\rm St} = 150 \left(\frac{\dot{N}_{\rm ion}}{10^{50}\ {\rm s}^{-1}}\right)^{1/3} \left(\frac{n_s}{{\rm cm}^{-3}}\right)^{-2/3} {\rm pc}. \quad (12)$$

For $w > 1.5$, r_s depends on n_s more weakly ($\propto n_s^{-1/w}$) than $r_{\rm St}$ ($\propto n_s^{-2/3}$). As far as $r_{\rm St} < r_s$, as is the case in the initial stage of expansion, the I-front is of D-type. As the shock propagates and n_s decreases, $r_{\rm St}$ eventually overtakes r_s and the I-front changes into R-type.

Denoting the radius at which $r_{\rm St}$ is equal to r_s by $r_{\rm eq}$, the necessary condition for the transition into the R-type front within the lifetime of the central star is $r_{\rm eq} < l_{\rm D}$, namely,

$$M_{\rm halo} < M_{\rm crit}^{\rm ion}, \quad (13)$$

where

$$M_{\rm crit}^{\rm ion} = 5.0 \times 10^6 \left(\frac{l_{\rm D}}{270\ {\rm pc}}\right)^{3-(9/2w)} \left(\frac{\dot{N}_{\rm ion}}{10^{50}\ {\rm s}^{-1}}\right)^{(3/2w)} \times \left(\frac{1+z_c}{20}\right)^{3-(9/w)} M_\odot. \quad (14)$$

Figure 7 shows the above critical mass for complete ionization, adopting $v_{\rm D} = 20$ km s^{-1} in equation (9). In our fiducial case with $M_{\rm star} = 200\ M_\odot$ ($\dot{N}_{\rm ion} = 2.6 \times 10^{50}$ s^{-1}, $t_{\rm life}$=2.2 Myr), $w = 2$, and $z_c = 20$, it yields $M_{\rm crit}^{\rm ion} = 2.5 \times 10^6\ M_\odot$. Indeed, it agrees with our simulation results over a wide range of parameters.

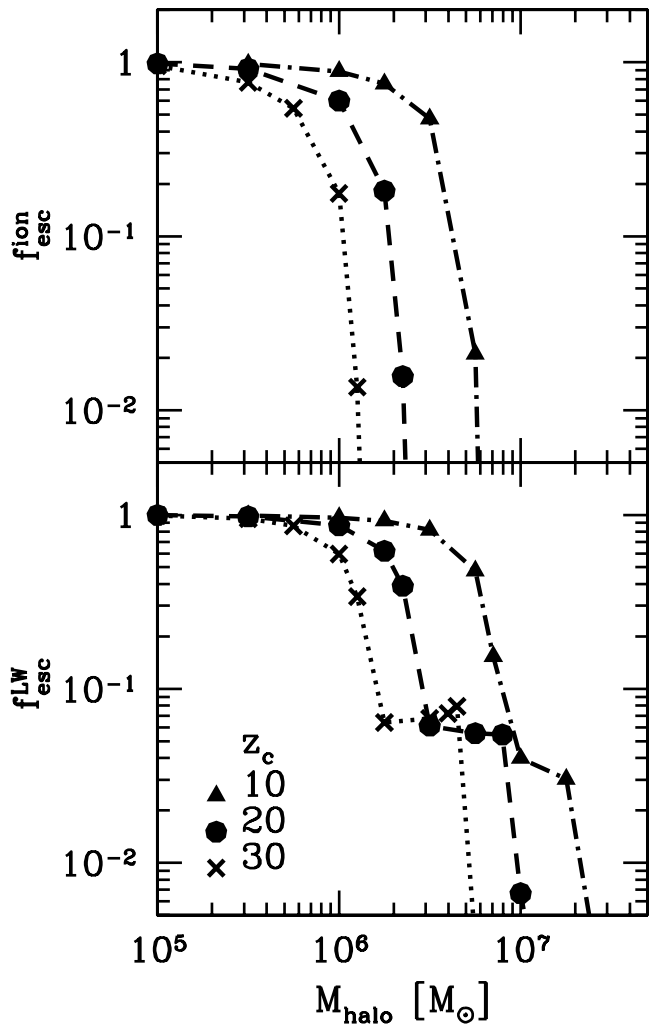

FIG. 6.—Same as Fig. 4, except that symbols denote collapse redshifts of $z_c = 10$ (*triangles*), 20 (*circles*), and 30 (*crosses*). [*See the electronic edition of the Journal for a color version of this figure.*]

If one is to estimate the critical mass for the escape of the LW photons separately, Figure 7 indicates that $M_{\rm crit}^{\rm LW} \sim 3M_{\rm crit}^{\rm ion}$ gives a reasonable fit to the simulation results for $w \simeq 2$. In the case of $80\ M_\odot \lesssim M_{\rm star} \lesssim 500\ M_\odot$, $10 \lesssim z_c \lesssim 30$, and $w = 2$, useful approximations for the critical masses are

$$M_{\rm crit}^{\rm ion} \sim 2.5 \times 10^6 \left(\frac{M_{\rm star}}{200\ M_\odot}\right)^{3/4} \left(\frac{1+z_c}{20}\right)^{-3/2} M_\odot, \quad (15)$$

$$M_{\rm crit}^{\rm LW} \sim 7.5 \times 10^6 \left(\frac{M_{\rm star}}{200\ M_\odot}\right)^{3/4} \left(\frac{1+z_c}{20}\right)^{-3/2} M_\odot, \quad (16)$$

where we have used a power-law fit to the results of Schaerer (2002), $\dot{N}_{\rm ion} \propto M_{\rm star}^{1.2}$ and $t_{\rm life} \propto M_{\rm star}^{-0.2}$, over the range $80\ M_\odot \lesssim M_{\rm star} \lesssim 500\ M_\odot$.

If helium is included in the calculation, the gas temperature will be higher by a factor of $\sim$2 for $T_{\rm eff} \sim 10^5$ K, because of an increase in the net heating rate (Abel & Haehnelt 1999). This will increase the shock velocity and consequently $l_{\rm D}$ in equation (9) by $\sim$40%. The critical mass $M_{\rm crit}$ will then become higher by $\sim$30% for $w = 2$.

3.4. *Effective Clumping Factor of Halos*

As an alternative way to quantify the strength of radiative feedback, we plot in Figure 8 the ratio $N_{\rm ion}/N_{\rm H}$ as a function of $M_{\rm star}$, w, and z_c, where $N_{\rm ion}$ is the total number of ionizing photons emitted by the central star and $N_{\rm H}$ is the total number of hydrogen atoms in a halo. In order for the ionizing photons to escape from halos ($f_{\rm esc}^{\rm ion} > 1\%$; *circles*), $N_{\rm ion}/N_{\rm H} > 10 \sim 100$ is required. The threshold values of $N_{\rm ion}/N_{\rm H}$ are rather insensitive to $M_{\rm star}$ but increase with w or z_c. The H_2 photodissociating photons can escape from halos ($f_{\rm esc}^{\rm LW} > 1\%$; *crosses and circles*) for $N_{\rm ion}/N_{\rm H} > 3 \sim 30$.

It is often assumed in the literature that $N_{\rm ion}/N_{\rm H}$ needs to be higher than the clumping factor $\langle n^2\rangle/\langle n\rangle^2$ for the gas to be completely ionized. While this assumption is likely to be valid for nearly uniform media, it cannot be applied to the present case, in which the density gradient is large. To see this point more clearly, we also display in Figure 8 the *effective* clumping factor of the halo in its initial configuration for $3/2 < w < 3$:

$$C_{\rm halo} = \langle n_i^2\rangle_{\rm halo}/\langle n_i\rangle_{\rm halo}^2 = \frac{(3-w)^2}{3(2w-3)}\left(\frac{1}{x^{2w-3}} - 1\right)\frac{1-x^3}{(1-x^{3-w})^2}, \quad (17)$$

where $\langle\ \rangle_{\rm halo}$ denotes the volume average taken at $r_{\rm in} \le r \le r_{\rm vir}$ and $x = r_{\rm in}/r_{\rm vir}$. The initial condition of the present simulations (eq. [7]) gives

$$x = \left[3.93 \times 10^{-7}\left(\frac{1+z_c}{20}\right)^3\right]^{1/w}. \quad (18)$$

Over the ranges of parameters studied in this paper, $C_{\rm halo}$ increases with increasing w and decreasing z_c. The dependence of $C_{\rm halo}$ on z_c is simply a product of our choice of $r_{\rm in}$ (eq. [7]). We have checked that our simulation results are not sensitive to the specific value of $r_{\rm in}$ (or x), while $C_{\rm halo}$ is.

Figure 8 shows that the halos are completely ionized and photons can escape from them even for $N_{\rm ion}/N_{\rm H} < C_{\rm halo}$. The dependences of $C_{\rm halo}$ on w and z_c do not agree with those of the threshold values of $N_{\rm ion}/N_{\rm H}$ for $f_{\rm esc}^{\rm ion} > 1\%$ either. These are the consequences of the enhanced ionization induced by the gas evacuation and the subsequent R-type I-front propagation. We stress that it is essential to incorporate the dynamical effects properly, as in equation (14), to account for ionization of the halo with a steep density gradient.

3.5. *Gas Evacuation and the Evolution of the Relic* H II *Regions*

The H II regions around a massive short-lived star embedded in a steep density medium never settle into a static Strömgren state. The I-front keeps expanding outward after the central star turns off. The relic H II regions then start cooling by recombination and inverse Compton cooling at such high redshifts, and the ionized fraction rapidly decreases while the outer part is still expanding. It is therefore meaningful to investigate how much gas is driven out of a halo in the end. In the cosmological context, dark matter halos continue growing, so it is likely that the expelled gas eventually falls back into the halo by gravitational force.

Figure 9 shows the evolution of the baryon fraction within $r_{\rm vir}$ in the cases of $M_{\rm halo} = 10^5$ and $10^6\ M_\odot$ in our fiducial runs. The halo gas is almost completely evacuated by $t = 2$ Myr for

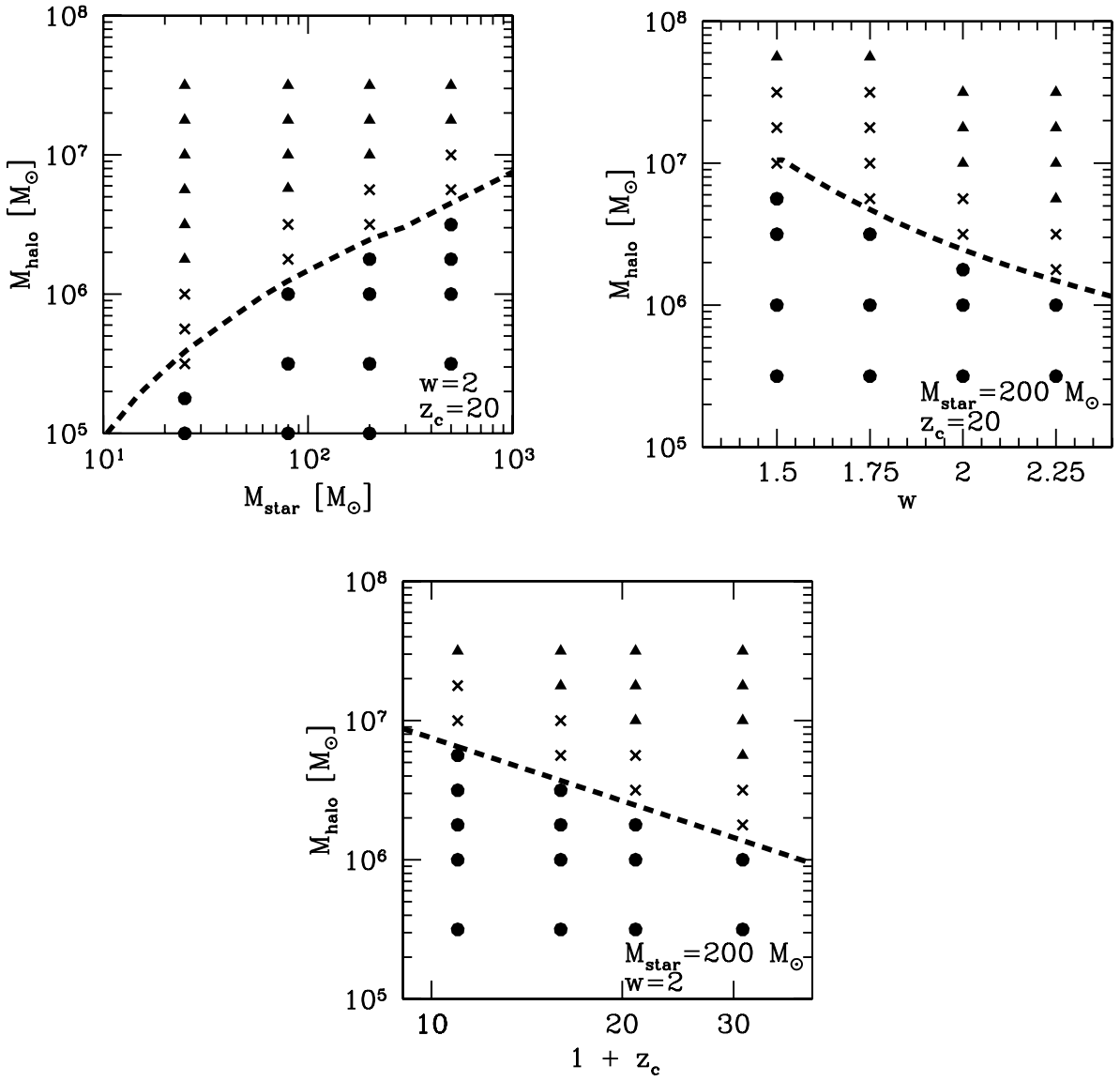

FIG. 7.—Critical masses of escape fractions as a function of $M_{\rm star}$, w, and z_c. Circles denote $f_{\rm esc}^{\rm ion} > 1\%$ and $f_{\rm esc}^{\rm LW} > 1\%$, crosses $f_{\rm esc}^{\rm ion} < 1\%$ and $f_{\rm esc}^{\rm LW} > 1\%$, and triangles $f_{\rm esc}^{\rm ion} < 1\%$ and $f_{\rm esc}^{\rm LW} < 1\%$. Dashed lines indicate the analytic estimation for the critical mass scale of complete ionization (eq. [14]). [*See the electronic edition of the Journal for a color version of this figure.*]

$M_{\rm halo} = 10^5\ M_\odot$. For $M_{\rm halo} = 10^6\ M_\odot$, on the other hand, the gas mass fraction slightly increases by gas accretion during the first few million years. This is simply because the shock radius is $\sim$70 pc at $t = 2$ Myr, still inside the virial radius (Fig. 3). Even after the central star fades away, the gas will maintain its outward motion until it dissipates kinetic energy. The baryon fraction rapidly decreases at $\sim$5 Myr, when the shock front overtakes the virial radius.

We have further carried out the runs with the same set of parameters as those in Figure 9 but omitting the radiation force term in equation (2). While the radiation force enhances the outward momentum of the gas at small radii (Figs. 1 and 2), it helps little to evacuate the gas from a halo; the baryon fraction within $r_{\rm vir}$ is unchanged to within 5% when the radiation force is turned off.

If the central Population III star is so massive that they collapse directly to form a black hole (see, e.g., Fryer et al. 2001), it does not disturb the gas mechanically any more. The ultimate fate of the expelled gas is then described in simple terms. The cooled gas does not provide hydrodynamic pressure in the relic H II region, and thus at least some fraction of the gas eventually falls back toward the halo center (i.e., gravitational potential well) after a while, gaining roughly a free-fall velocity. The free-fall time for a halo collapsing at $z = 15$ is $t_{\rm ff} \sim 50$ Myr in our adopted ΛCDM cosmology. The host halo itself is growing in mass, but the growth timescale is also of the order $t_{\rm ff}$. It is thus clear that the subsequent star formation is possible only after this fallback of the gas happens, i.e., gas condensation at the halo center begins only after a few times 10^7 yr. Note also that the evolution is more complicated when the central star explodes as a supernova. In such cases, the halo gas may be swept up by the supernova blast wave.

4. COSMOLOGICAL IMPLICATIONS

4.1. *Suppression of Star Formation*

The internal feedback due to photodissociation of hydrogen molecules by radiation from the very first star likely prohibits further star formation within the same halo (Omukai & Nishi

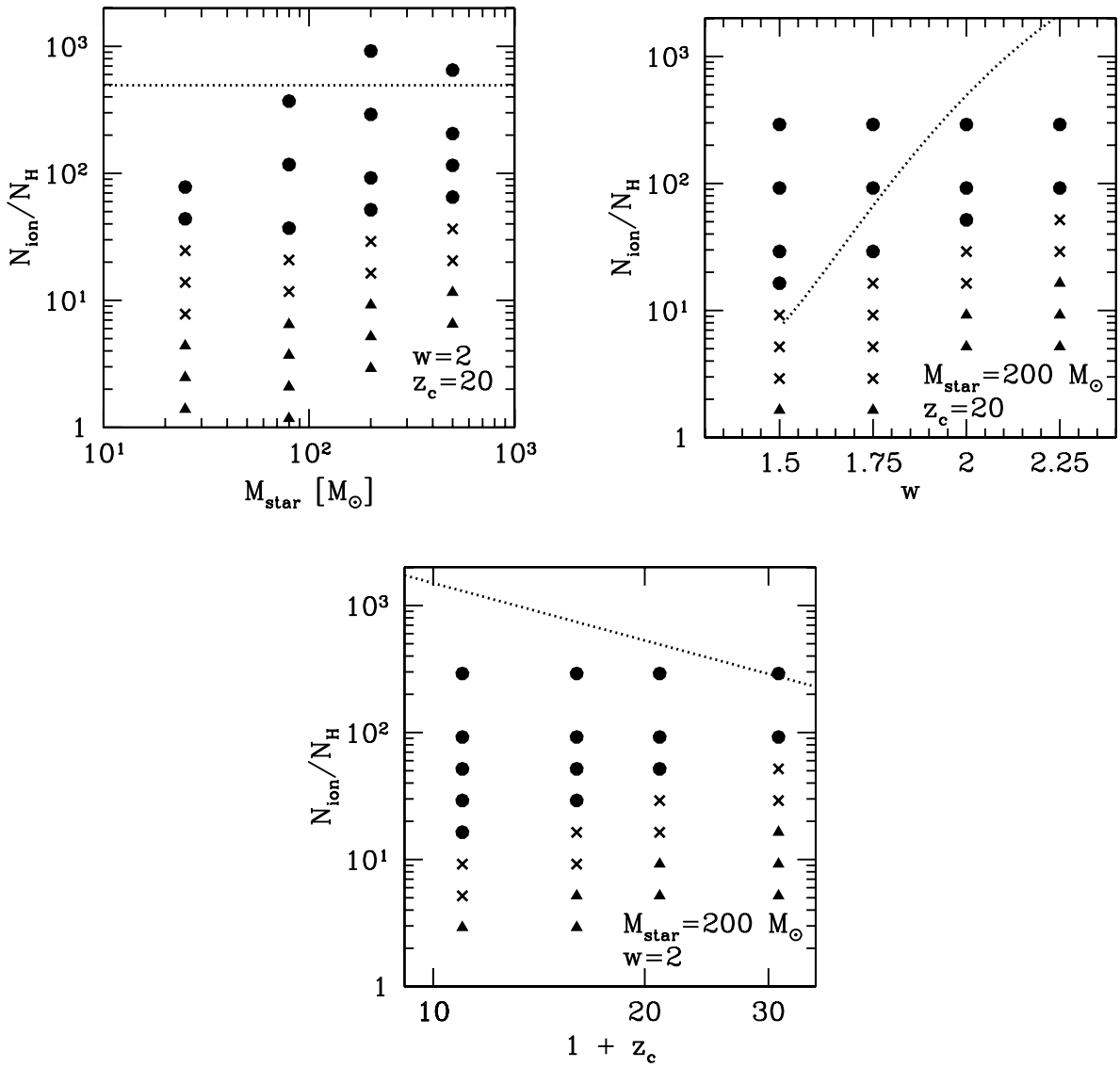

FIG. 8.—Total number of ionizing photons emitted from the central star per hydrogen atom in a halo as a function of $M_{\rm star}$, w, and z_c. Meanings of the symbols are the same as in Fig. 7. Also plotted for reference by dotted lines are the effective clumping factor of the halo $C_{\rm halo}$ defined in the main text. [*See the electronic edition of the Journal for a color version of this figure.*]

1999). Our results (Figs. 4–6) provide a reasonable estimation for the critical halo mass that determines the efficiency of the internal feedback in terms of $f_{\rm esc}^{\rm LW}$. As shown in § 3, early star formation via H_2 cooling will be self-regulated internally and suppressed in halos with $M_{\rm halo} \lesssim 10^7 M_\odot$. For such small halos, $f_{\rm esc}^{\rm LW}$ is high and the "one star-per-halo" assumption adopted in the present paper is likely to be adequate. For halos with sufficiently larger mass and lower $f_{\rm esc}^{\rm LW}$, the multiple formation of stars or star clusters could take place. Therefore, while the very first stars are likely to form in low-mass halos (Abel et al. 2002; Bromm et al. 2002), the subsequent star formation may be suppressed until slightly larger mass systems begin to collapse. The latter systems may dominate the cosmic star formation rate and metal production at high redshifts (e.g., Ricotti et al. 2002).

Note that our results are not restricted by the underlying one-star-per-halo assumption. We have shown that the emitted number of ionizing photons, not the number of stars itself, is a key parameter to control the photon escape fraction (see eq. [14]). Given a weak variation of the main-sequence lifetime with mass, values of $M_{\rm star}$ above $\sim$100 $M_\odot$ can be interpreted as the *total mass* of stars with nearly Eddington luminosities; the case of a single 500 $M_\odot$ star is almost equivalent to that of a few 200 $M_\odot$ stars. Our results can therefore be rescaled and applied to a wider range of stellar numbers.

4.2. *Reionization of the Universe*

The present results on the evolution of H II regions may have profound implications for reionization of the universe. First, high values of photon escape fractions in low-mass halos imply that such halos can be a major site of photon production, at least in the early phase of reionization. In order to surpass recombination at $z = 20$, the emission rate of ionizing photons per unit comoving volume must be higher than $\dot{n}_{\rm ion} = 3.4 \times 10^{51} C_{\rm IGM}$ s^{-1} Mpc^{-3}, where $C_{\rm IGM}$ is the clumping factor of the IGM (eq. [26] of Madau et al. 1999). This can be achieved if the comoving number of halos hosting a 200 $M_\odot$ star is greater than $13 C_{\rm IGM}$ Mpc^{-3}. In the absence of heavy metals, gas can condense to form stars by H_2 cooling only in halos above the mass $M_{\rm H_2} \simeq 5 \times 10^5\ h^{-1}\ M_\odot$ (Fuller & Couchman 2000; Yoshida et al. 2003a). The number of halos just above $M_{\rm H_2}$, expected from the Press & Schechter (1974)

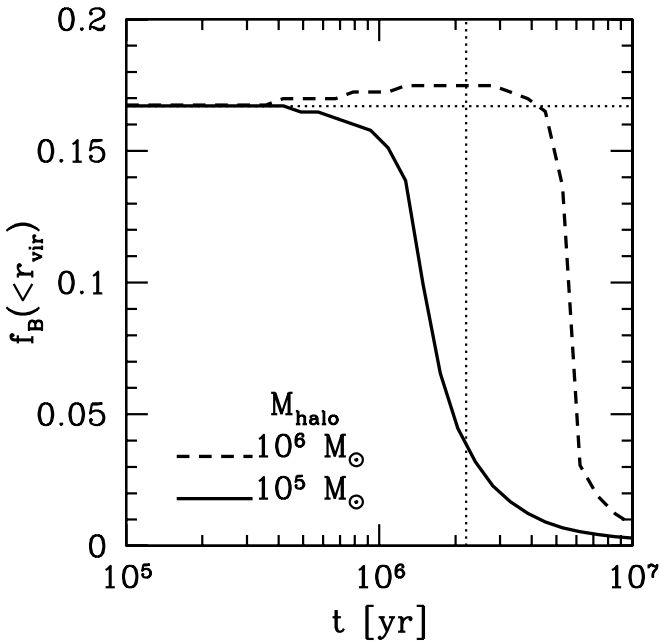

FIG. 9.—Evolution of baryon fraction within virial radius for $M_{\rm halo} = 10^5\ M_\odot$ (*solid lines*) and $10^6\ M_\odot$ (*dashed lines*) in our fiducial runs. Dotted lines denote the lifetime of the central star (*vertical*) and the universal baryon fraction Ω_B/Ω_M (*horizontal*). [*See the electronic edition of the Journal for a color version of this figure.*]

mass function, is $\sim$30 Mpc^{-3} at $z = 20$ in the conventional ΛCDM model with $(\Omega_M, \Omega_\Lambda, h, \Omega_B, \sigma_8) = (0.3, 0.7, 0.7, 0.05, 0.84)$. The number of low-mass halos is thus comparable to that needed to ionize the IGM for a moderate value of $C_{\rm IGM}$. As mentioned below, however, the photon production rate will be significantly suppressed once secondary feedback effects start to operate.

Second, given the sharp decline in photon escape fractions with increasing halo mass (Figs. 4–6), there remains only a narrow range of halo mass in which Population III stars can form and contribute to reionization. The photon production can therefore be stalled readily as the star formation in the low-mass halos is suppressed by, for instance, the rise in the external UV radiation field (e.g., Machacek et al. 2001; Kitayama et al. 2001; Yoshida et al. 2003a; Oh & Haiman 2003) and the mechanical energy input from supernovae (e.g., Ricotti & Ostriker 2004a). The photon emission may also decline as the transition from Population III to Population II stars takes place as a result of metal enrichment (Cen 2003; Mackey et al. 2003; Bromm & Loeb 2003). Because of high recombination rate at high redshifts, the ionized fraction may even start decreasing after a brief period of star formation in minihalos. This can probably last until a considerable number of stars form in larger systems. We will investigate these points more quantitatively in a future publication.

Finally, evacuation of the halo gas by the central star may further delay the formation of miniquasars that are suggested to be alternative reionization sources in the early universe (e.g., Madau et al. 2004; Ricotti & Ostriker 2004b). Such reionization models usually assume efficient gas accretion onto central black holes that are the remnants of very massive ($M_{\rm star} > 300\ M_\odot$) Population III stars. Our calculations, however, indicate that initial gas accretion would be very inefficient for the black hole remnants that formed in small-mass ($<10^6\ M_\odot$) halos, because the halo gas is effectively evacuated in the first place, and, indeed, the gas continues moving outward for over 10^7 yr after the central star dies. Similar arguments hold for the formation of the second-generation stars. It remains to be seen whether or not early reionization inferred by the *WMAP* data is achieved in models with these ionizing sources.

4.3. *Supernova Feedback*

Mechanical feedback from the first stars is often cited as a destructive process in the context of early structure formation. If the mass of the central star lies in the range $140\ M_\odot < M_{\rm star} < 260\ M_\odot$, it will explode as an energetic supernova via pair-instability mechanism (Barkat et al. 1967; Bond et al. 1984; Fryer et al. Heger 2001; Heger & Woosley 2002). It is also suggested that the observed abundance of metal-poor halo stars can be accounted for by a "hypernova" with progenitor mass $20\ M_\odot < M_{\rm star} < 130\ M_\odot$ (Umeda & Nomoto 2002, 2003). In either case, the energy released can be as large as $\sim 10^{53}$ erg, which is much larger than the gravitational binding energy of a minihalo with mass $\sim 10^6\ M_\odot$.

At the first sight, this simple argument appears to support the notion that high-z supernovae are enormously destructive. However, the evolution of the *cooling* supernova remnants (SNRs) crucially depends on the properties of the surrounding medium, particularly on the central density after the gas is redistributed by radiation. Our simulations showed that the final gas density at the halo center is primarily determined by the host halo mass. For small-mass halos that are almost completely ionized by a massive star, the central gas density reduces to ~ 1 cm^{-3}. A large fraction of the supernova explosion energy will then be converted into the kinetic energy of the ambient media. On the other hand, for the larger mass halos, the central gas density exceeds 10^4 cm^{-3}. Most of the explosion energy will be quickly radiated away via free-free emission and the inverse Compton scattering of the CMB photons. The free-free emission from the hot ($T \sim 10^6$–10^8 K) SNR leads to soft X-ray emission. It has been suggested that positive feedback, in terms of molecular hydrogen formation, is possible if an early X-ray background builds up (Haiman et al. 2000; Oh 2002; Venkatesan et al. 2001; see, however, a counterargument by Machacek et al 2003). Population III supernova remnants are therefore among the most plausible X-ray sources in the early universe (Yoshida et al. 2004). We will study in detail the evolution of the SNR and the X-ray emission efficiency in a forthcoming paper.

5. CONCLUSIONS

We have studied the structure and the evolution of early cosmological H II regions formed around the first stars. In particular, we addressed how efficiently the central stars ionize the gas in low-mass halos with $M_{\rm halo} = 10^5$–$10^8\ M_\odot$ collapsing at $z_c = 10$–30. We showed that a single massive star can ionize all the halo gas in a few million years if the host halo mass is smaller than a few million solar masses. The final ionization fraction of the halo gas depends sensitively on the initial gas-density profile as well as the host halo mass. While a few previous cosmological simulations suggest an approximately isothermal density profile ($\rho \propto r^{-2}$) around the first star-forming regions, the exact slope may vary among the primordial gas clouds. We therefore carried out a number of simulations for plausible cases and explored a large parameter space. For a similar set of parameters, our results are in good agreement with those of Whalen et al. (2004), who studied the case of $M_{\rm halo} = 7 \times 10^5\ M_\odot$ and $z_c \sim 20$.

The formation of the H II region is characterized by initial slow expansion of a weak D-type ionization front near the center, followed by rapid propagation of an R-type front throughout the outer gas envelope. We find that the transition between the two front types is indeed a critical condition for the complete ionization of halos of cosmological interest. This accounts for the fact that the photon escape fraction has a sharp transition from ~100% to ~0% at a certain critical mass scale of 10^6–10^7 $M_\odot$. It is also responsible for the fact that the whole halo can be ionized under smaller values of photon-to-baryon ratio than the effective clumping factor. The radiation force can contribute to enhancing the outward motion within ~30 pc at the initial stage of expansion.

Based on the obtained numerical results, we developed an analytic model to predict the escape fractions of ionizing photons and dissociating photons. We find that there is a narrow range of halo mass in which Population III stars can form and contribute to ionizing the universe, provided that low-mass halos are in infall phases and host a small number of massive stars. The analytic model and the numerical results presented in this paper provide useful ingredients for the studies of early reionization, the evolution of high-redshift supernova remnants, and the formation of the second-generation stars.

We thank Tom Abel, S. Peng Oh, and Kazuyuki Omukai for fruitful discussions, and the referee for useful comments. N. Y. acknowledges support from the Japan Society of Promotion of Science Special Research Fellowship (02674). This work is supported in part by the grants-in-aid from the Ministry of Education, Science and Culture of Japan (14740133:TK, 15740122:HS, and 16002003:MU).

APPENDIX A

IMPLEMENTATION OF RADIATIVE TRANSFER

Above the Lyman limit of hydrogen ($h\nu \geq 13.6$ eV), we solve the following radiative transfer equation taking account of both absorption and emission:

$$\frac{dI_\nu}{ds} = -n_{\rm H\,I}\sigma_\nu I_\nu + j_\nu, \tag{A1}$$

where I_ν is the specific intensity at frequency ν, s is the distance along a light ray, σ_ν is the photoionization cross section of hydrogen (Osterbrock 1989), and j_ν is the local emission coefficient for ionizing radiation. In the case of $kT \ll h\nu_{\rm L}$ as in the present simulations, j_ν is given by (Tajiri & Umemura 1998; Susa & Umemura 2000)

$$j_\nu = \begin{cases} \dfrac{h\nu\alpha_1 n_e n_{\rm H\,II}}{4\pi\delta\nu} & \nu_{\rm L} \leq \nu < \nu_{\rm L} + \delta\nu, \\ 0 & \nu \geq \nu_{\rm L} + \delta\nu, \end{cases} \tag{A2}$$

where $\nu_{\rm L}$ is the Lyman limit frequency, α_1 is the recombination rate to the ground state of hydrogen (Osterbrock 1989), and $\delta\nu = kT/h$ is the thermal width of the recombination line. Recombinations to the excited states are excluded in equation (A2) because they are unable to produce ionizing photons above the Lyman limit. In practice, equation (A1) is solved separately for $\nu_{\rm L} \leq \nu < \nu_{\rm L} + \delta\nu$ and $\nu \geq \nu_{\rm L} + \delta\nu$. For the latter, photoionization is regarded as pure absorption and the solution reduces to

$$I_\nu(s) = I_\nu(0)\exp(-\sigma_\nu \mathcal{N}_{\rm H\,I}), \quad (\nu \geq \nu_{\rm L} + \delta\nu), \tag{A3}$$

where $\mathcal{N}_{\rm H\,I} = \int_0^s n_{\rm H\,I} ds'$ is the column density of neutral hydrogen along the photon path.

The coefficient (per unit time) and the heating rate (energy per unit time per unit volume) for photoionization of hydrogen atoms ($\mathrm{H} + h\nu \rightarrow e^- + \mathrm{H}^+$) are then given respectively by

$$k_{\rm ion} = \int d\Omega \int_{\nu_{\rm L}}^\infty d\nu \frac{I_\nu \sigma_\nu}{h\nu}, \tag{A4}$$

$$\mathcal{H} = n_{\rm H\,I} \int d\Omega \int_{\nu_{\rm L}}^\infty d\nu \frac{I_\nu \sigma_\nu}{h\nu}(h\nu - h\nu_{\rm L}), \tag{A5}$$

where the integral with respect to Ω is taken over all solid angles. Assuming that the momentum of a photon is transferred to the gas upon each ionization, the radiation force per unit mass in the direction specified by a unit vector $\boldsymbol{n}$ is expressed as

$$f_{\rm rad}(\boldsymbol{n}) = \frac{X_{\rm H\,I}}{m_p c} \int d\Omega \int_{\nu_{\rm L}}^\infty d\nu\, I_\nu \sigma_\nu \cos\theta, \tag{A6}$$

where θ is the angle between $\boldsymbol{n}$ and the light ray, m_p is the proton mass, and c is the speed of light. In our spherically symmetric simulations, $\boldsymbol{n}$ lies in the radial direction. Photon momentum carried away by reprocessed radiation is properly taken into account by using the solutions of multifrequency radiative transfer mentioned above.

As far as only the radiation from a central star is concerned, the intensity integrated over solid angles is well approximated at $\nu \geq \nu_{\rm L} + \delta\nu$ by

$$\int I_\nu d\Omega \simeq \int I_\nu \cos\theta d\Omega = \frac{L_\nu \exp\left(-\sigma_\nu \mathcal{N}_{\rm H\,I}\right)}{4\pi r^2}, \tag{A7}$$

where L_ν is the stellar luminosity, and r is the radial distance from the center, taken to be sufficiently larger than the physical size of the star.

On the other hand, the diffuse radiation just above the Lyman limit, $\nu_{\rm L} \leq \nu < \nu_{\rm L} + \delta\nu$, comes from all the directions. For the diffuse component, we directly solve equation (A1) by means of an impact parameter method (Mihalas & Weibel-Mihalas 1984). At each radial point, angular integrations in equations (A4)–(A6) are done over at least 20 bins in $\theta = 0 - \pi$. This is achieved by handling 400–1,000 impact parameters for light rays.

In the LW (11.2–13.6 eV) band, we use the self-shielding function of Draine & Bertoldi (1996) to compute the coefficient (per unit time) for photodissociation of H_2 molecules ($H_2 + h\nu \rightarrow H + H$):

$$k_{\rm H_2} = 0.15 \xi_{\rm pump} \chi f_{\rm shield}, \tag{A8}$$

where

$$\xi_{\rm pump} \simeq 3 \times 10^{-10}\ s^{-1}, \tag{A9}$$

$$\chi = \frac{\left(\nu/c \int I_\nu d\Omega\right)_{\nu/c=1000\ \text{Å}}}{4 \times 10^{-14}\ \text{ergs cm}^{-3}} \simeq \frac{\left(\nu L_\nu / 4\pi c r^2\right)_{\nu/c=1000\ \text{Å}}}{4 \times 10^{-14}\ \text{ergs cm}^{-3}}, \tag{A10}$$

$$f_{\rm shield} = \min\left[1, \left(\frac{\mathcal{N}_{\rm H_2}}{10^{-14}\ \text{cm}^{-2}}\right)^{-0.75}\right], \tag{A11}$$

and $\mathcal{N}_{\rm H_2}$ is the column density of H_2.

We also compute the coefficients for photodetachment of H^- ($H^- + h\nu \rightarrow e^- + H$) and photodissociation of H_2^+ ($H_2^+ + h\nu \rightarrow H^+ + H$) from the radiation below $\nu_{\rm L}$ as

$$k_i = \int d\Omega \int_{\nu_i}^{\nu_{\rm L}} d\nu \frac{I_\nu \sigma_{i,\nu}}{h\nu} \simeq \frac{1}{4\pi r^2} \int_{\nu_i}^{\nu_{\rm L}} d\nu \frac{L_\nu \sigma_{i,\nu}}{h\nu}, \tag{A12}$$

where the subscript i stands for H^- or H_2^+ and $\sigma_{i,\nu}$ denotes the cross section. For photodetachment of H^-, we use a fitting formula by Tegmark et al. (1997) to the cross section of Wishart (1979) with the low-energy cut-off $h\nu_{\rm H^-} = 0.74$ eV. For photodissociation of H_2^+, we use the cross section from Table 2 of Stancil (1994) down to $h\nu_{\rm H_2^+} = 0.062$ eV. Our results are insensitive to specific values of the low-energy cut-off, because blackbody spectra of stellar sources diminish at low energies. The radiation above $\nu_{\rm L}$ is also irrelevant since it will be heavily absorbed by hydrogen atoms whenever H^- and H_2^+ processes become relevant.

APPENDIX B

CODE TEST

We have tested and verified the accuracy of our Lagrangian code by a variety of test problems, such as the shock-tube problem, the Sedov explosion problem (Sedov 1959), and a comparison with the self-similar solution for the adiabatic accretion of collisional gas (Bertschinger 1985). We here describe the results of a "Strömgren sphere" test, which is the most relevant to the present paper.

We simulate the propagation of an I-front around a central source with $\dot{N}_{\rm ion} = 3.3 \times 10^{50}\ \text{s}^{-1}$ and $T_{\rm eff} = 10^4$ K in a uniform medium with $n_{\rm H} = 1\ \text{cm}^{-3}$. The Strömgren radius is at $r_{\rm St} = 220$ pc for $T = 10^4$ K. For the sake of direct comparison with analytic solutions, we exclude the radiation force and gravitational force terms from the momentum equation (eq. [2]). Figure 10 shows the radial profiles of hydrogen density, temperature, H I and H_2 fractions, and the gas velocity. In contrast to the cases with steep density gradient ($w > 3/2$), the I-front is initially R-type at $r < r_{\rm St}$ and then changes into D-type at $r > r_{\rm St}$. The I-front is resolved with more than 10 gas shells. As in Figure 1, there temporally appears a thin shell of H_2 just in front of the H II region.

In Figure 11 we also plot the evolution of the I-front radius. For definiteness, we define it as the radius at which H I fraction is equal to 0.1. Also plotted for reference are the analytic solutions of I-front propagation in stationary and dynamical media (eqs. [12–9] and [12–20] of Spitzer 1978) for the photoheated temperature of $T = 10^4$ K. They are expected to describe the evolution of R-type and D-type fronts, respectively. Our simulation results in fact reproduce both of them within 5% accuracy at $t > 10^3$ yr. This further ensures the capability of the code for the simulations in the present paper.

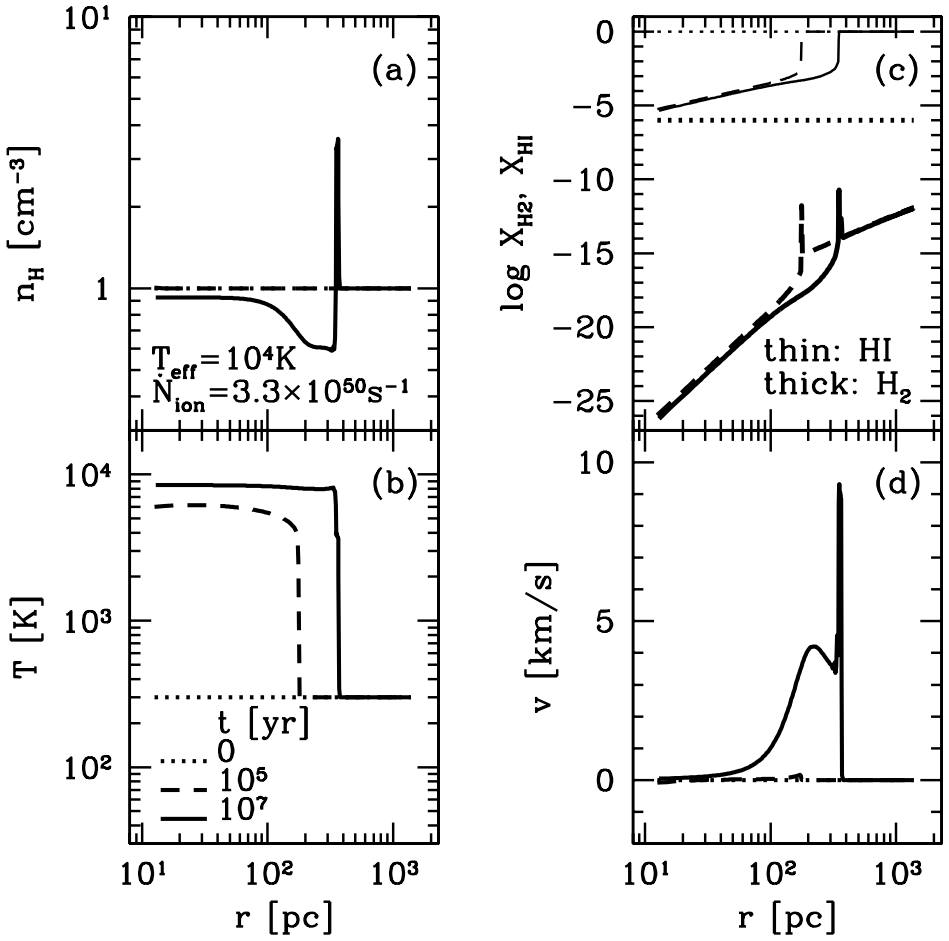

FIG. 10.—Propagation of an I-front in a uniform medium around a source with $\dot{N}_{\rm ion} = 3.3 \times 10^{50}$ s^{-1} and $T_{\rm eff} = 10^4$ K. Radial profiles are shown at $t = 0$ (*dotted lines*), 10^5 yr (*dashed lines*), and 10^7 yr (*solid lines*) for (*a*) hydrogen density, (*b*) temperature, (*c*) H I (*thin lines*) and H_2 (*thick lines*) fractions, and (*f*) radial velocity. The Strömgren radius is at $r_{\rm St} = 220$ pc. [*See the electronic edition of the Journal for a color version of this figure*.]

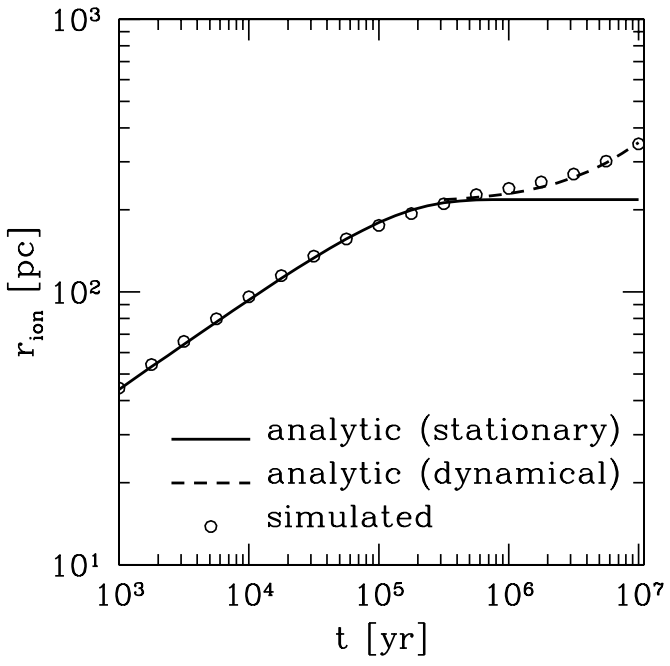

FIG. 11.—Evolution of an I-front in the simulation shown in Fig. 10 (*circles*). Lines denote the analytic solutions for the I-front propagation in stationary (*solid*) and dynamical (*dashed*) media described in the text. [*See the electronic edition of the Journal for a color version of this figure*.]

REFERENCES

Abel, T., Anninos, P., Norman, M. L., & Zhang, Y. 1998, ApJ, 508, 518
Abel, T., Bryan, G. L., & Norman, M. L. 2002, Science, 295, 93
Abel, T., & Haehnelt, M. G. 1999, ApJ, 520, L13
Barkana, R., & Loeb, A. 1999, ApJ, 523, 54
Barkat, Z., Rakavy, G., & Sack, N. 1967, Phys. Rev. Lett., 18, 379
Bertschinger, E. 1985, ApJS, 58, 39
Bond, J. R., Arnett, W. D., & Carr, B. J. 1984, ApJ, 280, 825
Bond, J. R., Szalay, A. S., & Silk, J. 1988, ApJ, 324, 627
Bowers, R. L., & Wilson, J. R. 1991, Numerical Modelling in Applied Physics and Astrophysics (Boston: Jones and Bartlett)
Bromm, V., Coppi, P. S., & Larson, R. B. 2002, ApJ, 564, 23
Bromm, V., & Loeb, A. 2003, Nature, 425, 812
Bromm, V., Yoshida, N., & Hernquist, L. 2003, ApJ, 596, L135
Bullock, J., et al. 2001, MNRAS, 321, 559
Caramana, E. J., Shashkov, M. J., & Whalen, P. P. 1998, J. Comp. Phys., 144, 70
Cen, R. 2003, ApJ, 591, 12
Couchman, H. M. P., & Rees, M. J. 1986, MNRAS, 221, 53
Draine, B. T., & Bertoldi F. 1996, ApJ, 468, 269
Efstathiou, G. 1992, MNRAS, 256, 43
Franco, J., Tenorio-Tagle, G., & Bodenheimer, P. 1990, ApJ, 349, 126
Fryer, C. L., Woosley, S. E., & Heger, A. 2001, ApJ, 550, 372
Fukugita, M., & Kawasaki, M. 1994, MNRAS, 269, 563
Fuller, T. M., & Couchman, H. M. P. 2000, ApJ, 544, 6
Galli, D., & Palla F. 1998, A&A, 335, 403
Gnedin, N. Y., & Ostriker, J. P. 1997, ApJ, 486, 581
Haiman, Z., Abel, T., & Rees, M. J. 2000, ApJ, 534, 11
Haiman, Z., Rees, M. J., & Loeb, A. 1996, ApJ, 467, 522
———. 1997, ApJ, 476, 458
Haehnelt, M. G. 1995, MNRAS, 273, 249
Heger, A., & Woosley, S. E. 2002, ApJ, 567, 532
Kepner, J. V., Babul, A., & Spergel, D. N. 1997, ApJ, 487, 61
Kitayama, T., & Ikeuchi, S. 2000, ApJ, 529, 615
Kitayama, T., Susa, H., Umemura, M., & Ikeuchi, S. 2001, MNRAS, 326, 1353
Kitayama, T., Tajiri, Y., Susa, H., Umemura, M., & Ikeuchi, S. 2000, MNRAS, 315, L1
Kogut, A., et al. 2003, ApJS, 148, 161
Machacek, M. E., Bryan, G. L., & Abel, T. 2001, ApJ, 548, 509
———. 2003, MNRAS, 338, 273
Mackey, J., Bromm, V., & Hernquist, L. 2003, ApJ, 586, 1
Madau, P., Haardt, F., & Rees, M. J.,1999, ApJ, 514, 648
Madau, P., Rees, M. J., Volonteri, M., Haardt, F., & Oh, S. P. 2004, ApJ, 604, 484
Mihalas, D., & Weibel-Mihalas, B. 1984, Foundations of Radiation Hydrodynamics (Oxford: Oxford Univ. Press)
Nakamura, F., & Umemura, M. 2002, ApJ, 569, 549
Navarro, J. F., Frenk, C. S., & White, S. D. M. 1997, ApJ, 490, 493
Oh, S. P. 2002, ApJ, 569, 558
Oh, S. P., & Haiman, Z. 2003, MNRAS, 346, 456
Omukai, K., & Inutsuka, S. 2002, MNRAS, 332, 59
Omukai, K., & Nishi, R. 1999, ApJ, 518, 64
Osterbrock, D. E. 1989, Astrophysics of Gaseous Nebulae and Active Galactic Nuclei (Mill Valley: University Science Books)
Press, W. H., & Schechter, P. 1974, ApJ, 187, 425
Rees, M. J. 1986, MNRAS, 218, 25
Ricotti, M., Gnedin, N. Y., & Shull, J. M. 2001, ApJ, 560, 580
———. 2002, ApJ, 575, 33
Ricotti, M., & Ostriker, J. P. 2004a, MNRAS, 350, 539
———. 2004b, MNRAS, 352, 547
Ricotti, M., & Shull, J. M. 2000, ApJ, 542, 548
Schaerer, D. 2002, A&A, 382, 28
Sedov, L. I. 1959, Similarity and Dimensional Methods in Mechanics (New York: Academic)
Shapiro, P. R., & Giroux, M. L. 1987, ApJ, 321, L107
Shapiro, P. R., Iliev, I. T., & Raga, A. C. 2004, MNRAS, 348, 753
Shapiro, P.R. Iliev, I.T., Raga, A.C., & Martel, H. 2003, in AIP Conf. Proc. 666, The Emergence of Cosmic Structure (Melville: AIP), 89
Shu, F. H., Lizano, S., Galli, D., Cantó, J., & Laughlin, G. 2002, ApJ, 580, 969
Sokasian, A., Yoshida, N., Abel, T., Hernquist, L., & Springel, V. 2004, MNRAS, 350, 47
Spergel, D.N., et al. 2003, ApJS, 148, 175
Spitzer, L., Jr. 1978, Physical Processes in the Interstellar Medium (New York: Wiley)
Stancil, P. C. 1994, ApJ, 430, 360
Strömgren, B. 1939, ApJ, 89, 526
Susa, H., & Kitayama, T. 2000, MNRAS, 317, 175
Susa, H., & Umemura, M. 2000, ApJ, 537, 578
———. 2004, ApJ, 600, 1
Tajiri, Y., & Umemura, M. 1998, ApJ, 502, 59
Tegmark, M., Silk, J., Rees, M., Blanchard, A., Abel, T., & Palla, F. 1997, ApJ, 474, 1
Thoul, A. A., & Weinberg, D. H. 1995, ApJ, 442, 480
———. 1996, ApJ, 465, 608
Umeda, H., & Nomoto, K. 2002, ApJ, 565, 385
———. 2003, Nature, 422, 871
Umemura, M., & Ikeuchi, S. 1984, Prog. Theor. Phys., 72, 47
Venkatesan, A., Giroux, M., & Shull, J. M. 2001, ApJ, 563, 1
Wada, K., & Venkatesan, A. 2003, ApJ, 591, 38
Welter, G. L. 1980, ApJ, 240, 514
Whalen, D., Abel, T., & Norman, M. 2004, ApJ, 610, 14
Wishart, A. W. 1979, MNRAS, 187, 59P
Yorke, H. W. 1986, ARA&A, 24, 49
Yoshida, N., Abel, T., Hernquist, L., & Sugiyama, N. 2003a, ApJ, 592, 645
Yoshida, N., Bromm, V., & Hernquist, L. 2004, ApJ, 605, 579
Yoshida, N., Sokasian, A., Hernquist, L., & Springel, V. 2003b, ApJ, 591, L1